Wave Motion 129 (2024) 103348

Contents lists available at ScienceDirect

Wave Motion

journal homepage: www.elsevier.com/locate/wamot

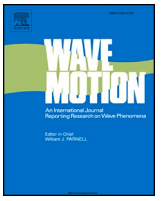

Bound states in the continuum for antisymmetric lamb modes in composite plates made of isotropic materials

Nan Gao [a], Ricardo Martin Abraham-Ekeroth [a,b,c], Daniel Torrent [a,*]

[a] Grup de Recerca óptica de Castelló (GROC), Institut de Noves Tecnologies de la Imatge (INIT), Universitat Jaume I, Castelló de la Plana, 12071, Spain
[b] Instituto de Física Arroyo Seco, Pinto 399, 7000 Tandil, Argentina
[c] Centro de Investigaciones en Física e Ingeniería del Centro de la Provincia de Buenos Aires (UNCPBA-CICPBA-CONICET), Campus Universitario, 7000 Tandil, Argentina

ARTICLE INFO

Keywords:
Bound states in the continuum
Lamb waves
Asymmetric elastic structures
Opto-mechanics
Elastic-wave BICs
Metamaterial device prototyping

ABSTRACT

In this study, we report a numerical design and observation of bound states in the continuum (BICs) for Lamb waves. BICs for elastic-wave systems, especially in non-periodic configurations, are difficult to obtain due to their intricate polarization states. However, the study in this matter has become very important, especially in the field of opto-mechanics or other multi-field couplings at micro or nanoscales. To illustrate the design concept, we simulate the introduction of a piece of silica (SiO_2) into a thin infinite Si plate and show that, for specific aspect ratios, BICs for elastic waves can be predicted. We present numerical results for both two-dimensional (2D) rectangular plates and three-dimensional (3D) disk structures. Moreover, we also investigate the modal contributions of both the background and inclusion media during the occurrence of BICs, further verifying the physical background of our design strategy. Although we have focused our work on asymmetric Lamb modes, the current method can also be applied to construct other types of elastic-wave BICs, providing a powerful tool for metamaterial device prototyping based on the control or guiding of elastic waves.

1. Introduction

Bound states in the continuum (BICs), also known as trapped modes, are non-radiating localized modes that simultaneously coexist within the continuous spectrum of radiation waves [1,2]. The concept of BICs was first mathematically proposed in quantum mechanics [2] and has further attracted great interest over the last decade in many classical wave systems, such as electromagnetic [3-6], aero-acoustic [7-11], hydroacoustic [12,13], and elastic wave [14-18] structures. Generally, BICs are impossible to excite via external fields. However, it is feasible to obtain quasi-BICs (QBICs) with high but finite Q-factors by structural design. These QBICs are being widely used in optics and photonics owing to their high-Q resonances, such as sensors [19-21], lasers [4,22-25], filters [26,27], and nonlinearity generators [28-30].

In addition to optical BICs, acoustic BICs have also garnered significant attention. They were initially identified in 'plate-in-waveguide' systems while examining pressure enhancement near parallel plate gratings in a wind tunnel [1,31]. Subsequently, numerous studies have integrated acoustic resonance cavities to achieve different types of BICs, both theoretically and experimentally,

* Corresponding author.
E-mail address: dtorrent@uji.es (D. Torrent).

https://doi.org/10.1016/j.wavemoti.2024.103348
Received 24 January 2024; Received in revised form 14 April 2024; Accepted 7 May 2024
Available online 15 May 2024

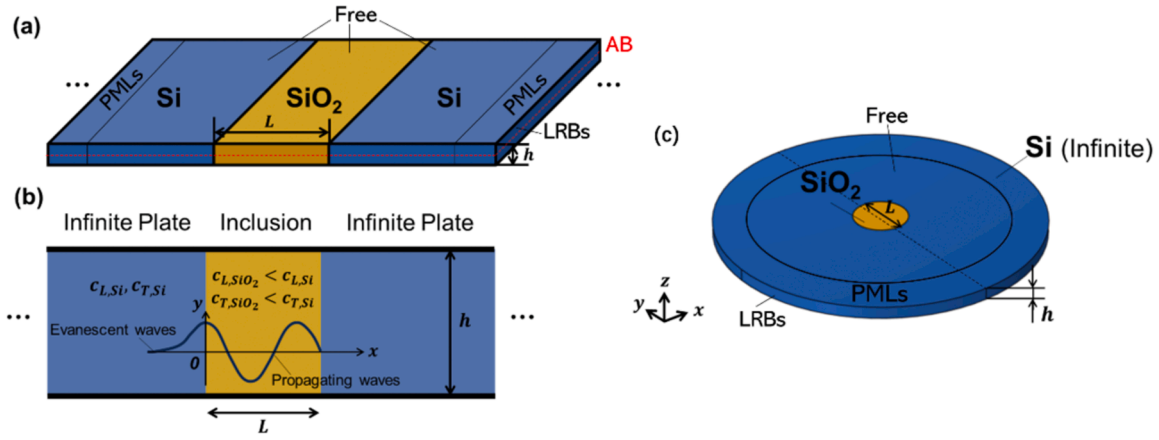

Fig. 1. Strategy to find BICs and Geometries considered in this work. (a) Perspective view of a thin infinite Si plate with a SiO_2 inclusion whose length is L. The height of the whole plate, h, is common to both media. (b) Simplified 2D model for (a), showing the constraints imposed to the eigenstates of the system to facilitate the appearance of BICs. (c) View of the geometry for the 3D problem of the disc with a central inclusion. The details of the methodology used are summarized in panels 1a and 1c.

including symmetry-protected (SP) BICs [9,32], Friedrich-Wintgen (FW) [10,11], and Fabry-Perot [33,34].

Compared to BICs in optics and acoustics, the research reported on elastic waves has been limited, primarily due to their intricate polarization states [35]. Nonetheless, the applications of elastic BICs have become promising for all fields working with mechanical oscillators [36], ultra-sensitive devices [37], and quantum information processors [38]. Some recent research has explored elastic BICs based on the coupling and transformation of elastic waves in different polarization directions [14-18]. Nevertheless, most of the latest work on elastic BICs is based on periodic structures with a certain symmetry and their practical implementation conditions are relatively constrained, particularly at small scales. Generally, the appropriate modeling of elastic BICs in non-periodical structures remains an open problem.

Here, we report antisymmetric trapped modes in 2D and 3D non-periodical Lamb wave systems, focusing the study on the lowest orders. We find that elastic BICs and QBICs can be constructed by introducing a solid, small inclusion into very thin plates if the former's material is "softer" than the latter's, i.e., the propagation velocities of the inclusion are lower than those for the outer medium. By using this combination of geometry and constitution the frequencies of such BICs can be easily tuned by changing the plate's thickness or the aspect ratio h/L, where h is the heigh of the composite plate and L is the width of inclusion.

In what follows, Section II briefly summarizes the method and the strategy to excite BICs based on total internal reflection. Section III is devoted to the results and discussion. Section IV concludes with a succinct recapitulation of the key features highlighted in this study.

2. Methods

2.1. BIC design-strategy

For acoustic or electromagnetic waveguides with an embedded cavity, BICs can be obtained by symmetry protection if the speed of the wave inside the inclusion is smaller than that in the waveguide. This mechanism can be illustrated if we consider a composite waveguide with a constant height, h. In such a case, the wavenumber in the transversal direction with respect to plate's main axis, $k_\perp$, is conserved inside and outside the "cavity". Then, the longitudinal wavenumber, which is the responsible for the propagation along the structure, is given by

$$k_\parallel = \sqrt{\frac{\omega^2}{c^2} - k_\perp^2} \tag{1}$$

where c is the wave velocity. If we choose c such that $k > k_\perp$, real values for $k_\parallel$ can be obtained which correspond to propagating waves along the composite plate or waveguide. Conversely, if c is chosen to make $k < k_\perp$, the resulting values for $k_\parallel$ are complex numbers so that they can be related to evanescent waves. By utilizing this design strategy, we can select the appropriate values for c inside and outside the inclusion to ensure propagating waves inside the insertion and evanescent outside, thereby obtaining localized states (BICs or QBICs).

BICs based on this mechanism can then be easily realized in acoustics and optics [39-41], where the vertical wavenumber $k_\perp$ is conserved in a waveguide with different materials. However, for guided elastic waves, this is not the case since in general a well-defined $k_\perp$ does not exist. The polarization conversion occurring in elastic is the responsible phenomenon for the non-conservation of the vertical wavenumber, so that all the plate modes are excited in the formation of the cavity. For a specific frequency range, only one of these modes, the A0, is propagative in the plate, and the geometrical parameters of the cavity can make

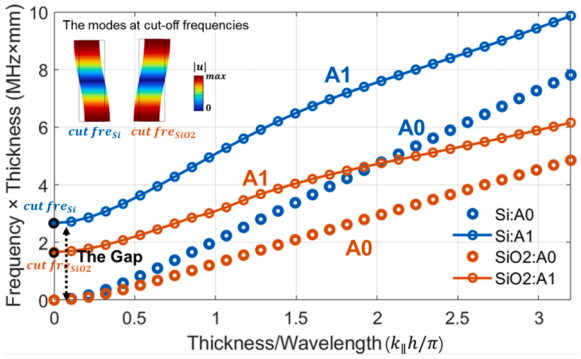

Fig. 2. Dispersion relations for the lowest modes in single-material plates. The plates are $h = 0.8$ mm in height. Blue [orange] curves for Si [SiO_2]. Circles [lines with circles] represent the A_0 [A_1] mode's dispersion in both single-material plates. The modes A_1 for each cut-off frequency are shown in the inset, where the colors indicate the absolute displacement value.

that the amplitude of this mode be zero in the formation of the cavity mode. When this happens, a BIC is formed.

With this strategy, we first consider constructing BICs on an infinitely thin plate. In this infinite structure, we assume for simplicity an inclusion of a solid, isotropic material as embedded in it, as shown in Fig. 1a and b. Here, we use Si as the host material for the plate, and SiO_2 for the inclusion (guest) since this material has lower elastic wave velocities than silicon's. In this work, we only consider BICs for the lowest-energy antisymmetric modes A_0 and A_1 as the research object. The study is then extended to azimuthal geometries to naturally complement and apply our results of the design method.

2.2. Simulation models

We perform simulations using the commercial finite-element software COMSOL Multiphysics 6.0. In the 2D configuration, Fig. 1a and b, we take a sufficiently long domain along the horizontal direction as the host material which sandwiches a rectangular inclusion of size L (Fig. 1a in perspective view). The height of the whole system is h. The main simulation details for each respective geometry can be seen in Fig. 1a and 1c, although the composite plate's problem is indeed modeled as a 2D geometry.

In the case of 3D simulations, an analogous symmetric structure is used, which consists of a disk of height h with a cylindrical inclusion of radius $L/2$ in its center (Fig. 1c). To save computational resources, half of the disk is used in the simulation runs by putting a symmetric condition for the displacement fields on the middle cut plane (dash line in Fig 1c), namely, $\overline{u}.\breve{n} = 0$, where $\overline{u}$ is the displacement vector and $\breve{n}$ is the unit normal vector of the considered sectional plane. In both 2D and 3D calculations, Si and SiO_2 are characterized by the values of Young's modulus, Poisson's ratio, and density as $E_{Si} = 170$ GPa, $\nu_{Si} = 0.28$, $\rho_{Si} = 2329$ kg/m^3, and $E_{SiO_2} = 63.8$ GPa, $\nu_{SiO_2} = 0.246$, $\rho_{SiO_2} = 2300$ kg/m^3, respectively. For simplicity, we fix $L = 5$ μm and sweep h from 0.1 L to L to calculate eigenvalues and analyze their evolution. As we are only interested in the antisymmetric modes of the structures, another condition is used to further half-cut the domains and make the runs computationally less expensive, namely, we implement an antisymmetric boundary condition (AB) at the plane (line in 1D) located in the middle of the plate, red dash line in Fig. 1a, namely, $\overline{u}.\breve{t} = 0$, where $\breve{t}$ is the unit tangent vector of the considered plane (line). Although not shown in Fig. 1(c) for a better visualization, we apply the same AB condition in the middle of the disk's thickness that is expressed as $\overline{u}.\breve{t}_1 = 0$ and $\overline{u}.\breve{t}_2 = 0$, where now mean the orthogonal two tangent versors that represent the corresponding plane in 3D. Details for the simulation settings are described in *Appendix A: Simulation details*.

3. Results and discussion

3.1. 2D geometries

Following the methodology stated, we then search for confined modes in the inclusion region with evanescent behavior in the host medium. The excitation of BICs in this composite plate can also be thought in terms of the modes from the single-material plates for the concerned materials. Fig. 2 shows the first two anti-symmetric modes' dispersion relations for single plates with thickness $h = 0.8$ mm. Specifically, the curves show the real part of the solutions obtained. Noteworthy, the cut-off frequency for the SiO_2's A_1 mode lies in the region between the frequencies for the modes A_0 and A_1 when $k_{\|} = 0$ in Si. We call this frequency interval as "gap" (Fig. 2). For frequencies lying in the gap, two cases can occur: 1) the frequency observed is higher than or equal to the cut-off frequency for SiO_2, and therefore both anti-symmetric modes A0 and A1 can be excited inside the inclusion, or 2), the observed frequency is lower than such cut-off frequency and then only the A0 mode can be excited in SiO2. In any case, only A0 can exist outside the inclusion as a propagative mode, since all the other modes will have a complex wavenumber $k_{\|}$, as shown schematically in Fig. 1b. If the cavity is designed in such a way that the amplitude of the A0 mode in Si is zero, and all the energy goes to the evanescent modes, this mode will be perfectly trapped within the cavity and no energy will be radiated towards the plate.

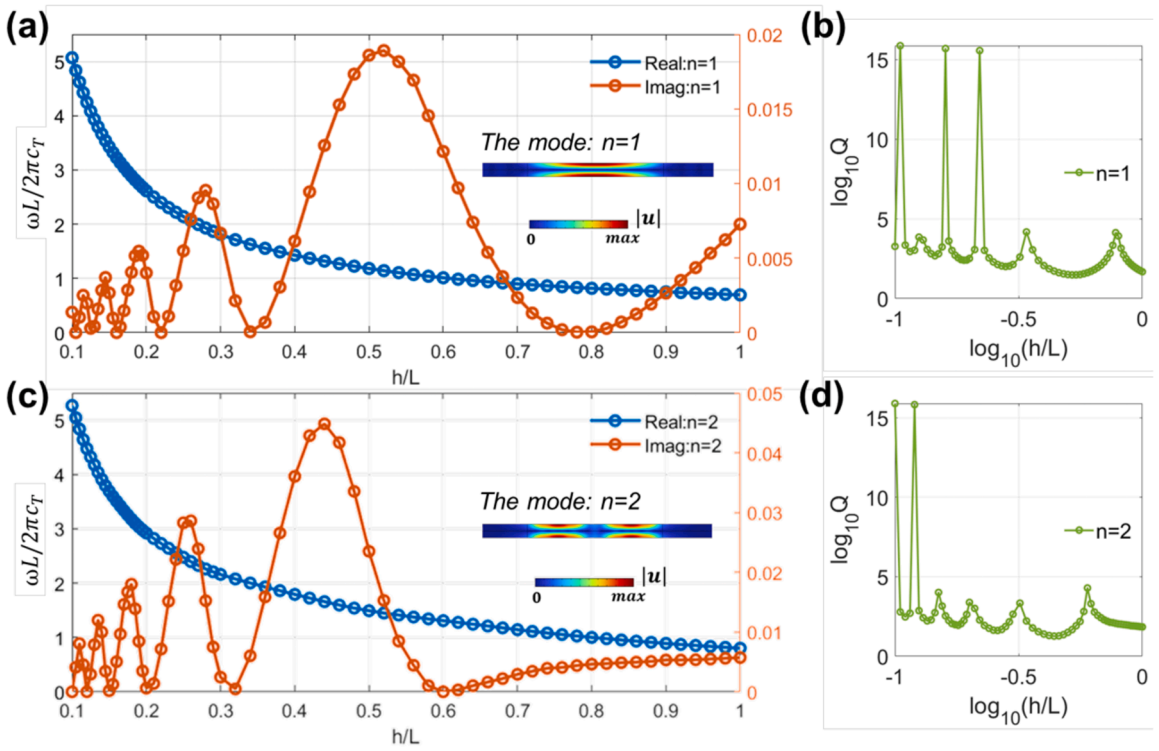

Fig. 3. Variation of the eigenfrequencies with the plate's aspect ratio. (a-b) [(c-d)] tracks the behavior of the mode $n = 1$ [$n = 2$]. Blue [orange] lines with circles in (a) and (c) represent the real [imaginary] part of the eigenvalues. Star symbols on the horizontal axis highlight the selected BIC cases. The displacement field distributions for these BICs are shown on the insets, with the colorbar representing their absolute value. Green lines in (b) and (d) denote the variation of the Q factor in $n = 1$, 2 states, where the axes are all in 10-based logarithmic scale.

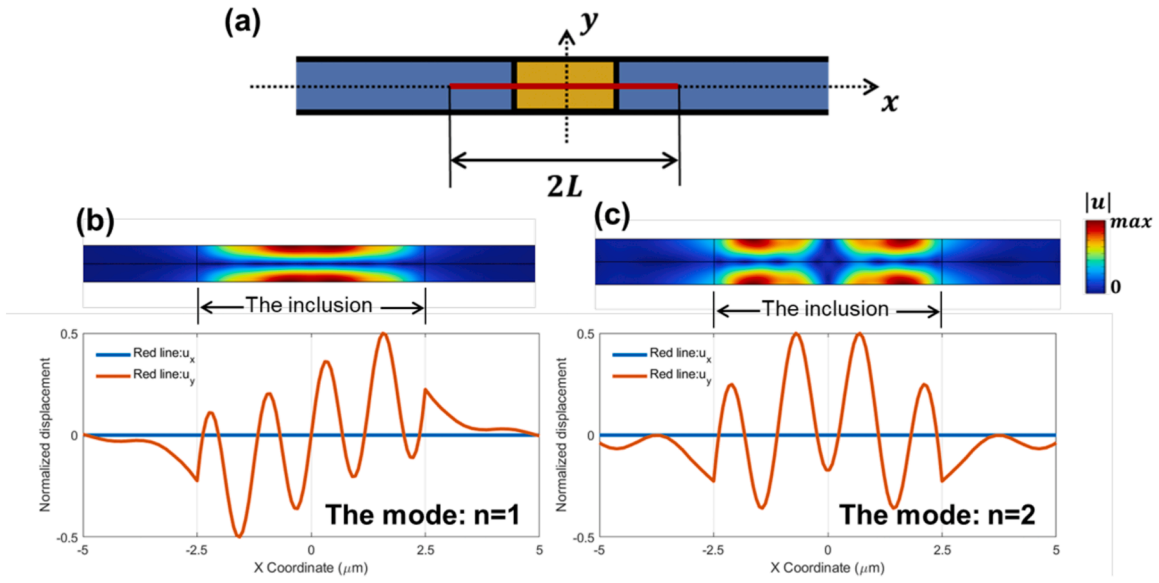

Fig. 4. Displacement distribution along the median line for the selected BICs (indicated with stars in Fig. 3a, c). (a) Schematic of the median line (indicated with the red line); transversal (u_y) and longitudinal (u_x) displacement distribution for (b) $n = 1$ with $h/L = 0.16$ and (c) $n = 2$ with $h/L = 0.2$.

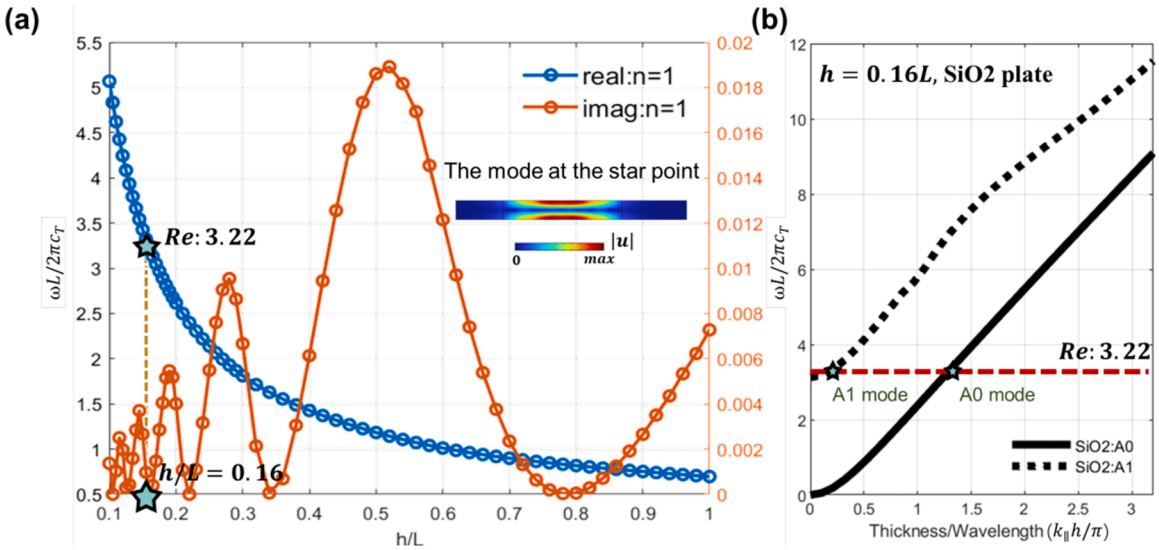

Fig. 5. Modal Analysis. We choose the BIC with $n = 1$ and $h/L = 0.16$ whose properties are shown in Figs. 3a and 4a. (a) Projecting the star point; the mode's dimensionless eigenfrequency is $\omega' = \frac{\omega L}{2\pi c_T} = 3.22$. (b) Dispersion relation for the modes A_0 and A_1 of the infinite SiO_2 plate with $h = 0.16L$. Solid and dash lines represent A_0 and A_1, respectively. The red (horizontal) dash line corresponding to ω' intersects with A_1 and A_0 at the two points represented by the green stars, which means that the first two antisymmetric modes of infinite SiO_2 plate are excited at ω'.

The cut-off frequencies for the asymmetric modes of Lamb waves can be expressed as [41]:

$$f_{cut} = \frac{(m+0.5)\times c_T}{2h}, m = 0,1,2\ldots \quad \text{foroddsolutions},$$
$$f_{cut} = \frac{n\times c_L}{2h}, n = 1,2,3\ldots \quad \text{forevensolutions}, \tag{2}$$

where c_T denotes the transverse wave velocity and c_L represents the longitudinal one. Based on Eq. (2), if the cut-off frequency of the inclusion needs to be lower than that of the host, then both c_T and c_L of the inclusion's material should be lower than those of host, which is the reason why we chose Si-SiO_2 as proof-of-concept materials, besides their current wide applications in opto-mechanics [42-48].

Fig. 3 shows a study corresponding to sweep the aspect ratio h/L over the structure. At this point it is necessary to define the discrete number n, which indicates the number of spots in one semi height region of the plate, e.g. $y > 0$ (see Fig. 4a). In this way, the lower order ($n = 1,\ 2$) antisymmetric modes of the structure can be picked out. In particular, the variation of their complex eigenvalues with the geometric parameter h/L is shown in Fig. 3a and c, where the blue and orange dotted lines represent the real and imaginary part of eigenvalues, respectively.

Results show that the real part of the eigenvalues decays exponentially with increasing thickness, while the imaginary part presents a sine-like oscillation, especially when the thickness is small. Under some specific values of h, the imaginary part can be close to or equal to 0, and the Q factor of the system, defined as $Q = \mathrm{Re}(fre)/(2\mathrm{Im}(fre))$, could be very high or even infinite, thus obtaining QBICs or BICs. The variations of Q with the geometry are shown in Fig. 3(b) and (d). From the distribution of Q factor, BICs can be obtained with $h/L \approx 0.105$, 0.16, and 0.2 ($\log_{10}(h/L) \approx -0.98$, -0.8, and -0.7 respectively) for $n = 1$, and with $h/L \approx 0.1$ and 0.12 ($\log_{10}(h/L) \approx -1$ and -0.92) for state $n = 2$. The geometrical parameters of the BICs appearing here lie in a very small range, thus more details for this study are presented in *Appendix B: The eigenvalues close to BICs*. Noteworthy, BICs only appear when the ratio h/L is small. In other words, under this design strategy, it is difficult to obtain QBIC/BIC for thick plates. Details for the case of thick plates are described in *Appendix C: The eigenvalues for thicker plates*.

To better explore the characteristics of these BICs, we select modes of points with zero imaginary parts when $n = 1$ and 2, as shown in Fig. 3a and b. For the $n = 1$ state, the displacement spots are concentrated at the center of the upper and lower surfaces of the half-simulated domain within the inclusion (inset in Fig. 3a); For $n = 2$, the spots are still on the upper and lower surfaces, but differentiated into two localized centers, symmetrically distributed around the (vertical) axis of symmetry (inset in Fig 3b).

The displacement distribution of the BICs' along the middle line (Fig. 4a, red line) shows in more detail that the modes are confined in the inclusion region; the propagating solution only exists in that region while outside the inclusion the solution corresponds to evanescent waves, which also confirms the feasibility of the design strategy outlined in Methods. Additionally, at the middle line (red line in Fig 4a), the longitudinal displacement (x direction) field is practically zero while the transversal displacement dominates. And it is clearly seen that the vibration is almost entirely localized within the inclusion; in other words, the amplitude in the host is much smaller than that in the inclusion. For displacement distribution along other paths, it can reflect more modal information of BICs, but they all reflect the same phenomenon, where vibration is concentrated at the inclusion. Details for the case of different path are

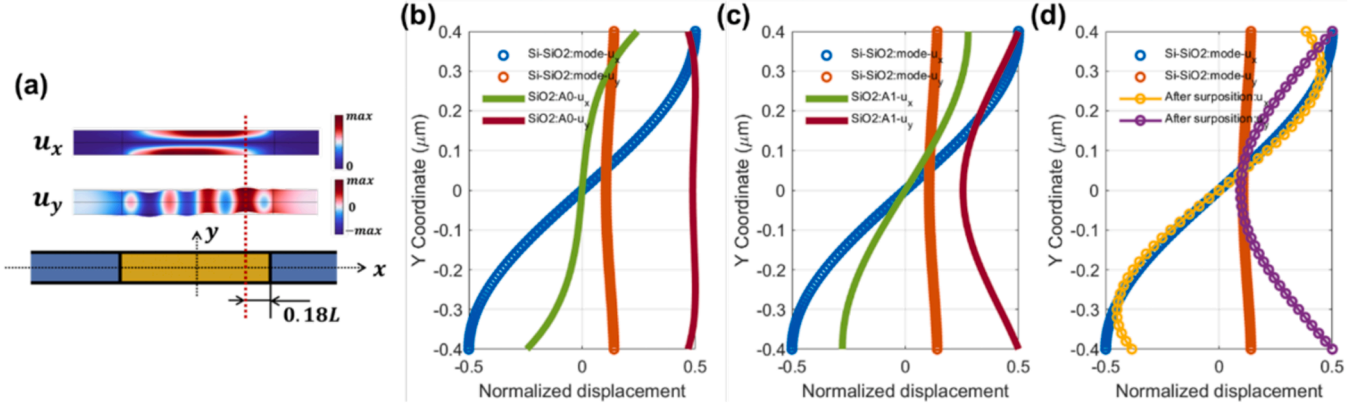

Fig. 6. Composition of a BIC in the inclusion region. (a) longitudinal (u_x) and transversal (u_y) displacement field for the selected BIC ($n = 1$, $h/L = 0.16$), the observed position inside the inclusion is indicated by the red dash line; (b)-(d) Comparison of u_x and u_y distributions between the Si-SiO_2 plate and (b) the A_0 mode, (c) the A_1 mode of an infinite SiO_2 plate and (d) after the superposition of these two modes. All the modes are normalized for convenience.

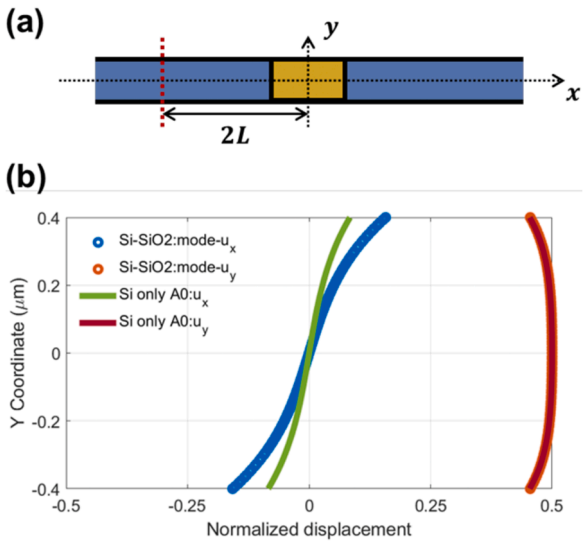

Fig. 7. Composition of BIC outside the inclusion region. (a) scheme showing the selected line to observe the field (indicated by the red dash line); (b) Comparison of u_x and u_y distributions between the Si-SiO_2 plate and the A_0 mode of an infinite Si plate.

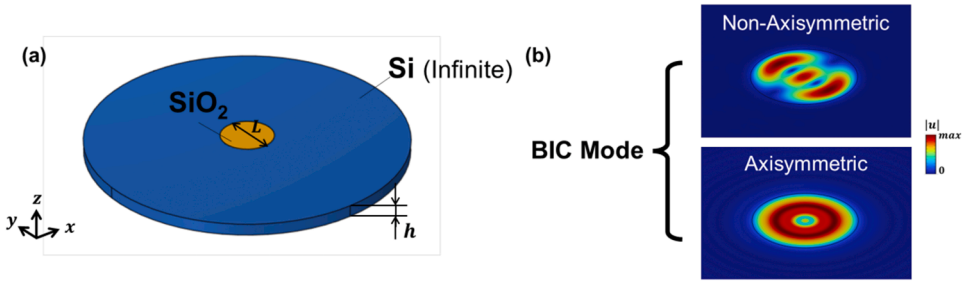

Fig. 8. Symmetry considerations for BICs in the 3D model. (a) Schematic diagram of an infinite Si plate with a circular SiO_2 inclusion; (b) The BICs are naturally divided into two types based on their symmetry, which consist of non-axisymmetric (top) and axisymmetric (bottom). The colormaps represent the absolute value of displacement field $|\vec{u}|$ in arbitrary units for two illustrative examples with different resonance frequencies.

described in *Appendix D: Displacement distribution for the selected BIC* ($y = h/4$).

To gain a deeper understanding for the mechanism of BICs mentioned above, it is necessary to explore the composition of anti-symmetric modes along the whole composite plate. Taking the BIC with $n = 1$ as an example, occurring at $h/L = 0.16$, its imaginary part is zero, and the dimensionless real part is exactly $\omega' = \omega L/2\pi c_T = 3.22$ (Fig. 5a). By corresponding the SiO_2 plate's dispersions in the low-order antisymmetric modes with ω', its excited modes A_0 and A_1 occur at the "spectral" positions indicated by green stars in Fig. 5b. Moreover, the longitudinal and transversal displacement fields of these modes can be linearly combined with a couple of constants (a, b) and further compare them with the displacement distribution at a BIC to see its composition, which can be expressed as

$$\begin{aligned} u_{x,Si-SiO_2} &= a u_{x,A0} + b u_{x,A1}, \\ u_{y,Si-SiO_2} &= a u_{y,A0} + b u_{y,A1}, \end{aligned} \tag{3}$$

where the subscripts x and y represent the longitudinal and transversal displacement fields of the modes, while the subscripts Si-SiO_2, A_0, and A_1 represent the composite plate, and the first two antisymmetric modes of the SiO_2 plate, respectively.

Now we select a special location, namely, 0.18 L away from the interface between the inclusion and the host ($x = 0.32L$), which is the antinode of the transversal displacement u_y of the BIC (Fig. 6a). The comparison of the normalized longitudinal and transversal displacements between the BIC and the inclusion' s A_0, A_1 modes is shown in Fig. 6b and c for each respective mode. Then, we tune the parameters (a, b) and compare the BIC with the mode obtained by superposition, and the BIC and both show a reasonable agreement at $(a, b) = (-0.8, 2)$, as displayed in Fig. 6c. The result shows that this BIC is composed of the superposition of A_0 and A_1 modes, and A_1 mode dominates. However, due to the finite size of SiO2 inclusion, the displacement field of BIC cannot perfectly match the superposition of A1 and A2 modes in an infinite SiO2 plate. The mismatch in Fig. 6d is caused by inclusion's boundaries.

Likewise, this method can be employed for the region outside the inclusion to examine its modal composition, shown as Fig. 7, where this time the antisymmetric modes of the Si plate are the ones to linearly combine to approach the general solution in Si. When$(a,$

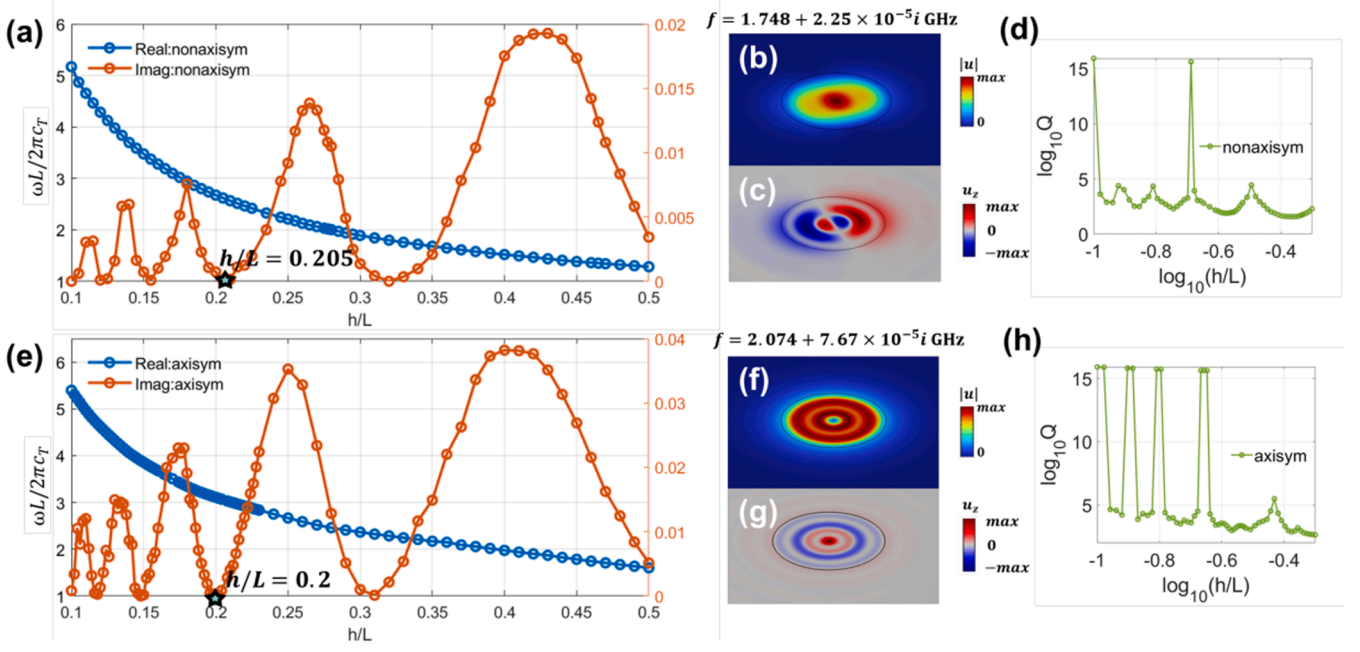

Fig. 9. Variation of the eigenfrequencies with the plate's aspect ratio in the 3D model. 3D model's eigenvalue with h/L, its eigenmodes are (a) non-axisymmetric and (e) axisymmetric, where the blue [orange] lines with circles represent the real [imaginary] part. (b), (f) Absolute value of the displacement field $|\overline{u}|$ [(c), (g) Transversal displacement field u_z] of the selected BICs (green stars in (a) and (b)). The colorbars of (b), (f) [(c), (g)] represent the absolute value [transversal component] of the total displacement field. The green lines in (d) and (h) denote the variation of Q in the selected non-axisymmetric and axisymmetric types, where the axes are all in 10-based logarithmic scale.

$b) = (1,0)$, the superposed mode matches well with the BIC's displacement field outside the inclusion. Under BIC, the mode outside the inclusion is only the A_0 of the substrate plate. This means that A_1 cannot propagate in the far field since it consists of evanescent waves. Moreover, even if there is an A_0 contribution outside the inclusion, its amplitude is very small, several orders of magnitude smaller than that inside the inclusion. For a better visualization, all the amplitudes have been normalized.

3.2. 3D geometries

Here we extend the 2D model to 3D, consisting of an infinite plate with a central circular inclusion of SiO_2, as shown in Fig. 8a. In the design and fabrication of optomechanical devices, the cylindrical structure is generally prevalent, making the exploration of BICs in this model more practical.

Due to the symmetry, its characteristic equations are more suitably expressed in cylindrical coordinates, so that the form of the solutions can be represented by Bessel functions [49]. Therefore, unlike the results of the 2D (rectangular) plate, the BICs of 3D circular plate can be further classified beyond the "energy" number n into two types, namely, axisymmetric, and non-axisymmetric (Fig. 8b). The former type is axisymmetric and can be ruled by a single discrete number as n (example in Fig. 8b bottom), while the latter is in addition characterized by angular modulation of their spots (top panel in Fig. 8b)

A study of variation of the eigenfrequencies with the aspect ratio h/L for this geometry is shown in the Fig. 9 for the lowest-energy modes The trends of the real and imaginary parts of the scaled eigenfrequencies ω', Fig. 9a and e are like those found for the 2D model. In the present case, we select two values close to $h/L \approx 0.2$ (from Fig. 9a and e, highlighted with green stars) to check their properties. As a non-axisymmetric mode, we found a BIC at $f = 1.748 + 2.5 \times 10^{-5}i$ GHz and $h/L = 0.205$ (Fig. 9a) whose displacement distribution is plotted in Fig. 9b and c. Its eigenmode can be seen from both components of the displacement field. Note that its vibration is almost entirely localized in the inclusion part, which together with its small imaginary part, $\mathrm{Im}(fre)$, defines this mode as a QBIC. Similarly, for the mode located at $h/L = 0.2$ in Fig. 9e, the imaginary part of its eigenvalue is 7.67×10^{-5} GHz, which results again very close to zero. From Fig. 9f and g, its axisymmetric nature can be observed; their spots are again mainly localized inside the inclusion region; thus, this is another type of QBIC. The behavior of the quality factors Q of these modes is also analyzed from Fig. 9d and h. The Q functions turn out to point several resonances; there are two peaks (two QBICs) for the non-axisymmetric type (Fig. 9d) and four peaks (four QBICs) for axisymmetric type (Fig. 9h), all of which appear under relatively small values of h/L.

These results confirm that our strategy to find elastic wave BICs can be applied to 2D as well as 3D structures, and further confirms its feasibility for applications.

4. Conclusions

In this work, we propose a strategy for finding or designing BICs that are based in the propagation of antisymmetric lamb modes along thin plates. The antisymmetric vibration can be localized successfully by introducing an inclusion made of a "softer" material than its host's. In particular, we illustrated this effect with examples based on composites plates made of Si-SiO_2, which showed that the propagating waves only exist inside the inclusion, while outside the inclusion the waves become evanescent. The present methodology can be applied to both 2D and 3D structures with high symmetry, which has been proved by our simulation results. The BICs in 3D cases turns out to be more complex, with two types of mode, namely, axisymmetric, and non-axisymmetric, but the variation of its complex eigenvalues with geometric parameters is like that found for the 2D model. Furthermore, we explored the composition of this kind of BICs in the lowest-energy region, with the result that the localized mode inside the inclusion seems to be always a combination of A_0 and A_1, while only A_0 is found outside the inclusion and with significantly lower amplitude. The results obtained in this work may provide reference for the structural design of BICs in elastic wave systems and fabrication of optomechanical devices in multiple applications concerning micro/nano scale.

CRediT authorship contribution statement

Nan Gao: Writing – original draft, Methodology, Investigation, Formal analysis. **Ricardo Martin Abraham-Ekeroth:** Writing – review & editing, Methodology, Investigation, Formal analysis, Conceptualization. **Daniel Torrent:** Writing – review & editing, Validation, Investigation, Funding acquisition, Formal analysis, Conceptualization.

Declaration of competing interest

The authors declare the following financial interests/personal relationships which may be considered as potential competing interests:

Daniel Torrent reports financial support was provided by University Jaume I. I am Editor of Wave Motion If there are other authors, they declare that they have no known competing financial interests or personal relationships that could have appeared to influence the work reported in this paper.

Data availability

No data was used for the research described in the article.

Acknowledgments

This research is supported by the DYNAMO project (101046489), funded by the European Union, but the views and opinions expressed are, however, those of the authors only and do not necessarily reflect those of the European Union or the European Innovation Council. Neither the European Union nor the granting authority can be held responsible for them. This publication is part of Project No. PID2021-124814NB-C22, funded by MCIN/AEI/10.13039/501100011033, "FEDER, A way of making Europe."

Supplementary materials

Supplementary material associated with this article can be found, in the online version, at doi:10.1016/j.wavemoti.2024.103348.

References

[1] C.W. Hsu, B. Zhen, A.D. Stone, J.D. Joannopoulos, M. Soljačić, Nat. Rev. Mater. 1 (2016) 1.
[2] J. von Neumann, E.P. Wigner, The collected works of Eugene Paul Wigner, Part A: Sci. Pap. (1993) 291.
[3] C.W. Hsu, B. Zhen, J. Lee, S. Chua, S.G. Johnson, J.D. Joannopoulos, M. Soljačić, Nature 499 (2013) 188.
[4] A. Kodigala, T. Lepetit, Q. Gu, B. Bahari, Y. Fainman, B. Kanté, Nature 541 (2017) 196.
[5] K. Koshelev, A. Bogdanov, Y. Kivshar, Sci. Bull. 64 (2019) 836.
[6] M. Minkov, I.A. Williamson, M. Xiao, S. Fan, Phys. Rev. Lett. 121 (2018) 263901.
[7] A. Lyapina, D. Maksimov, A. Pilipchuk, A. Sadreev, J. Fluid. Mech. 780 (2015) 370.
[8] L. Huang, et al., Nat. Commun. 12 (2021) 4819.
[9] B. Jia, L. Huang, A.S. Pilipchuk, S. Huang, C. Shen, A.F. Sadreev, Y. Li, A.E. Miroshnichenko, Phys. Rev. Appl. 19 (2023) 054001.
[10] S. Liu, S. Huang, Z. Zhou, P. Qian, B. Jia, H. Ding, N. Wang, Y. Li, J. Chen, Phys. Rev. Appl. 20 (2023) 044075.
[11] L. Huang, et al., Phys. Rev. Appl. 18 (2022) 054021.
[12] P. Cobelli, V. Pagneux, A. Maurel, P. Petitjeans, J. Fluid. Mech. 666 (2011) 445.
[13] M. Callan, C. Linton, D. Evans, J. Fluid. Mech. 229 (1991) 51.
[14] L. Cao, Y. Zhu, Y. Xu, S.-W. Fan, Z. Yang, B. Assouar, J. Mech. Phys. Solid. 154 (2021) 104502.
[15] B. Xia, Z. Jiang, L. Tong, S. Zheng, X. Man, Acta Mechanica Sinica 38 (2022) 521459.
[16] M. Martí-Sabaté, B. Djafari-Rouhani, D. Torrent, Phys. Rev. Res. 5 (2023) 013131.
[17] O. Haq, S. Shabanov, Wave Mot. 103 (2021) 102718.
[18] L. Cao, Y. Zhu, S. Wan, Y. Zeng, Y. Li, B. Assouar, Extrem. Mech. Lett. 47 (2021) 101364.
[19] D.N. Maksimov, V.S. Gerasimov, S. Romano, S.P. Polyutov, Opt. Expr. 28 (2020) 38907.
[20] Y. Wang, Z. Han, Y. Du, J. Qin, Nanophotonics 10 (2021) 1295.
[21] W. Yin, Z. Shen, S. Li, Y. Cui, F. Gao, H. Hao, L. Zhang, X.J.O.E. Chen, Opt. Expr. 30 (2022) 32162.
[22] K. Hirose, Y. Liang, Y. Kurosaka, A. Watanabe, T. Sugiyama, S. Noda, Nat. Photon. 8 (2014) 406.
[23] S.T. Ha, Y.H. Fu, N.K. Emani, Z. Pan, R.M. Bakker, R. Paniagua-Domínguez, A.I. Kuznetsov, Nat. Nanotechnol. 13 (2018) 1042.
[24] M.-S. Hwang, H.-C. Lee, K.-H. Kim, K.-Y. Jeong, S.-H. Kwon, K. Koshelev, Y. Kivshar, H.-G. Park, Nat. Commun. 12 (2021) 4135.
[25] Y.-G. Sang, J.-Y. Lu, Y.-H. Ouyang, H.-Y. Luan, J.-H. Wu, J.-Y. Li, R.-M. Ma, Nat. Commun. 13 (2022) 6485.
[26] L.L. Doskolovich, E.A. Bezus, D.A. Bykov, Photon. Res. 7 (2019) 1314.
[27] O. Kawachi, S. Mineyoshi, G. Endoh, M. Ueda, O. Ikata, E. Hashimoto, M. Yamaguchi, IEEE transactions on ultrasonics, Ferroelectr. Freq. Contr. 48 (2001) 1442.
[28] L. Carletti, K. Koshelev, C. De Angelis, Y. Kivshar, Phys. Rev. Lett. 121 (2018) 033903.
[29] K. Koshelev, Y. Tang, K. Li, D.-Y. Choi, G. Li, Y. Kivshar, ACS Photon. 6 (2019) 1639.
[30] X. Li, J. Ma, S. Liu, P. Huang, B. Chen, D. Wei, J. Liu, Light: Sci. Applic. 11 (2022) 317.
[31] R. Parker, J. Sound Vib. 4 (1966) 62.
[32] D. Evans, R. Porter, Q. J. Mech. Appl. Math. 51 (1998) 263.
[33] S. Hein, W. Koch, L. Nannen, J. Fluid. Mech. 692 (2012) 257.
[34] L. Huang, et al., Adv. Sci. 9 (2022) 2200257.
[35] K.F. Graff, Wave Motion in Elastic Solids, Courier Corporation, 2012.
[36] R. Riedinger, A. Wallucks, I. Marinković, C. Löschnauer, M. Aspelmeyer, S. Hong, S. Gröblacher, Nature 556 (2018) 473.
[37] A.G. Krause, M. Winger, T.D. Blasius, Q. Lin, O. Painter, Nat. Photon. 6 (2012) 768.
[38] A. Wallucks, I. Marinković, B. Hensen, R. Stockill, S. Gröblacher, Nat. Phys. 16 (2020) 772.
[39] P. Hu, C. Xie, Q. Song, A. Chen, H. Xiang, D. Han, J. Zi, Natl. Sci. Rev. 10 (2023) nwac043.
[40] M. Kang, T. Liu, C. Chan, M. Xiao, Nat. Rev. Phys. (2023) 1.
[41] Y. Lin, T. Feng, S. Lan, J. Liu, Y. Xu, Phys. Rev. Appl. 13 (2020) 064032.
[42] R. Van Laer, B. Kuyken, D. Van Thourhout, R. Baets, Nat. Photon. 9 (2015) 199.
[43] J. Bonhomme, M. Oudich, B. Djafari-Rouhani, F. Sarry, Y. Pennec, B. Bonello, D. Beyssen, P. Charette, Appl. Phys. Lett. 114 (2019).
[44] J. Chen, Y. Xiong, F. Xu, Y. Lu, Light: Sci. Applic. 10 (2021) 78.
[45] Y.A. Espinel, F.G. Santos, G.O. Luiz, T.M. Alegre, G.S. Wiederhecker, Sci. Rep. 7 (2017) 43423.
[46] D. Munk, M. Katzman, M. Hen, M. Priel, M. Feldberg, T. Sharabani, S. Levy, A. Bergman, A. Zadok, Nat. Commun. 10 (2019) 4214.
[47] W. Wang, Mater. (Basel) 15 (2022) 2484.
[48] M. Yan, J. Lu, F. Li, W. Deng, X. Huang, J. Ma, Z. Liu, Nat. Mater. 17 (2018) 993.
[49] A.W. Leissa, *Vibration of plates* (scientific and technical information division, Natl. Aeronaut. Space Administr. 160 (1969).